Supplementary Information (SI) for Inorganic Chemistry Frontiers.
This journal is © the Partner Organisations 2025

Supplementary Information for

Construction of V_2O_3/VN@GO Heterojunction Cathodes Derived from Polyoxovanadates for High-Performance Aqueous Zinc Ion Storage

Feng Gong[a], Wen-Fei Di[a], Yong-Jia Ding[a], Si-Yu Chen[a], Yun-Xiang Zhou[a], Rui Zhang[b,*], Dunmin Lin[a], Yu Huo[a, c*]

[a] College of Chemistry and Materials Science, Sichuan Normal University, Chengdu 610066, P. R. China

[b] School of Chemical and Environmental Engineering, Shanghai Institute of Technology, Shanghai, 201418, PR China

[c] Key Laboratory of Advanced Energy Materials Chemistry (Ministry of Education), Nankai University, Tianjin 300071, China

*E-mail: zhangrui-nadia@outlook.com (R. Zhang), huoyu@sicnu.edu.cn (Y. Huo)

Contents:

1. Experimental Section

1.1 Materials and methods

NH_4VO_3 (99%), $C_2H_8N_2$ (99%), CH_3OH (99.5%), and $Zn(CF_3SO_3)_2$ (98.0%) were all from Shanghai McLean Biochemical Technology Co. Acetylene were purchased form black Taiyuan Liyuan Lithium Battery Technology Center Co, Ltd. N-methylpyrrolidone (NMP, 99.9%), ethanol, polyvinylidene fluoride (PVDF)were all purchased form National Medicine Chemical Reagent Co, Ltd. Graphene oxide were purchased from Frontier Nano Materials Technology Co., Ltd.

X-ray powder diffraction (XRD) patterns of all samples were gained by a Miniflex diffractometer with Cu-Kα radiation (λ= 1.54 Å). The Fourier Transform infrared spectroscopy (FT-IR) were determined on a Bruker Vertex 70 IR spectrometer in the range of 400-4000 cm^{-1}. Thermogravimetric analysis (TGA) was performed on a NETZSCH STA 449 F5 thermogravimetric analyzer under nitrogen atmosphere at 6 °C min^{-1}. X-ray photoelectron spectroscopy (XPS, ESCALAB Xi) was carried out with an Al-Kα radiation source. The morphology and microstructure of the samples were analyzed by scanning electron microscopy (SEM, Zeiss/sigma 500) and transmission electron microscopy (TEM, JEOL JEM-2100 F). The electron paramagnetic resonance (EPR) spectrum was obtained using Bruker EMXplus.

1.2 Synthesis

1.2.1. Synthesis of $[(C_2N_2H_8)_4(CH_3O)_8V_8O_{12}]\cdot 4CH_3OH$ (V8)

V8 precursor was prepared according to the literature [1]. NH_4VO_3 (0.2257 g, 1.93 mmol), 15 mL methanol, and 450 μL ethanediamine were added successively into a 25 mL white Teflon-lined vessel and stirred thoroughly for ca. 2 h at RT and then heated at 100 °C for 3

days. After cooling to RT, black shuttle-shaped crystals of V8 were obtained after repeated washing with methanol, filtering, and drying.

1.2.2. Synthesis of V_2O_3/VN

V8 precursor (0.5 g) was put into a tube furnace and heated in the Ar atmosphere (99.999%) at 900 ℃ for 4 h with a heating rate of 5 ℃ min^{-1}, giving rise to the black powder product V_2O_3/VN (ca.0.46 g).

1.2.3. Synthesis of V_2O_3/VN@GO

Graphene oxide (0.02 g) was dissolved in 10 mL of deionized water and sonicated for 12 h to form a homogeneous solution, and then V_2O_3/VN product (0.1 g) was added and sonicated for another 30 min. The above solution was freeze-dried for three days to obtain V_2O_3/VN@GO.

1.3 Electrochemical tests

The active materials, acetylene black and PVDF were added to NMP at a mass ratio of 7:2:1 and stirred for 12 h, then the obtained slurry was coated on titanium foil and dried at 70 ℃ for 12 h in a vacuum oven, giving the cathode. The average active material loading was 1 mg cm^{-2}. The button cells (CR2032) were assembled in air with zinc foil as the anode, 3 M $Zn(CF_3SO_3)_2$ as the electrolyte, and glass fiber as the separator. The cyclic voltammetry curves (CV) and electrochemical impedance spectroscopy (EIS) were tested using the CHI 760E electrochemical workstation. Constant current charge-discharge tests were conducted on the battery automated testing system (LAND, CT2100A, Wuhan, China) in the voltage range of 0.2-1.6 V.

1.4 Measurements of galvanostatic intermittent titration (GITT)

The GITT test was carried out at a current density of 0.1 A g^{-1} with a constant current charge of 5 min and the relaxation of 10 min, respectively. The diffusion coefficient of zinc ions can be formulated as follows:

$$D = \frac{(4L^2\Delta E_s^2)}{(\pi\tau\Delta E_t^2)}$$

Where D stands for the ionic diffusion coefficient, L represents the thickness of the electrode, referring to the diffusion length of zinc ions, τ is the relaxation time of the current, ΔE_s and ΔE_t corresponds to the voltage changes caused by the charge and discharge of pulse and constant current, respectively [2].

2.Supplementary Characterization

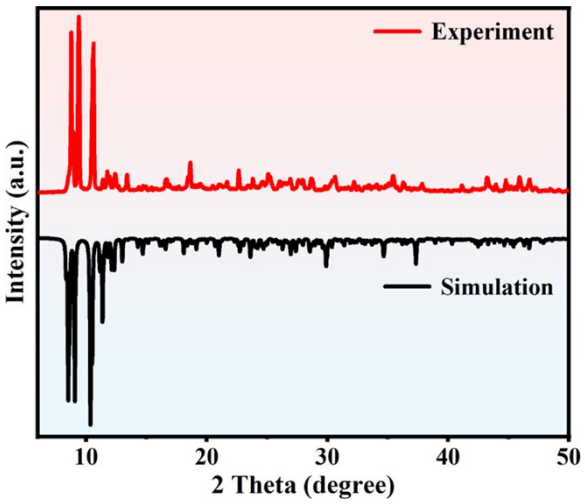

Figure S1. Experimental and simulated X-ray powder diffraction patterns for V8.

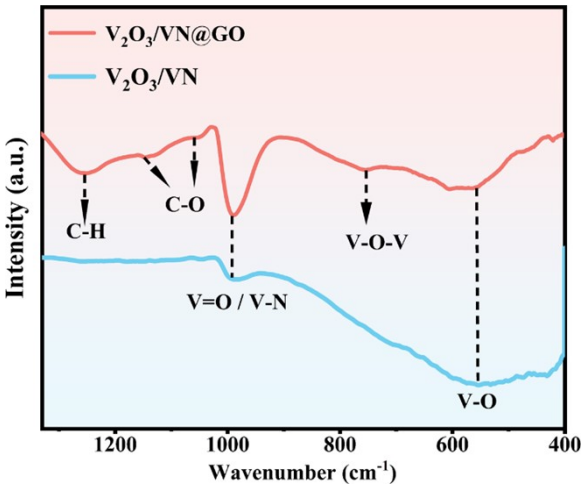

Figure S2. Fourier transform infrared of V_2O_3/VN@GO.

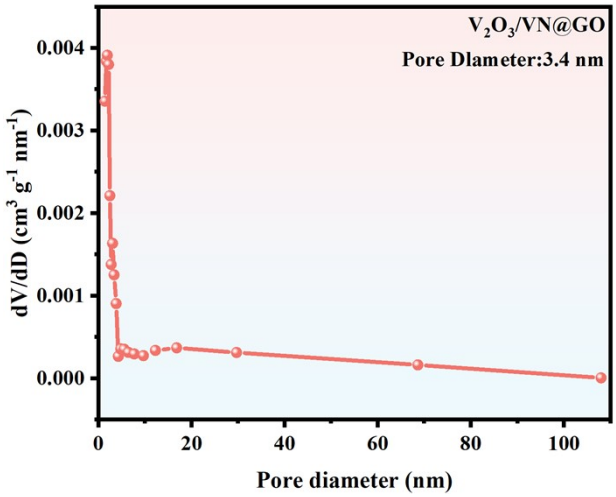

Figure S3 corresponding pore size distribution of V_2O_3/VN@GO.

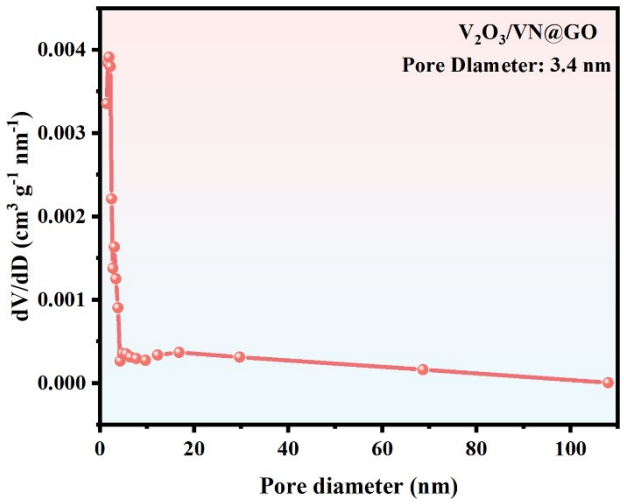

Figure S4 corresponding pore size distribution of V_2O_3/VN.

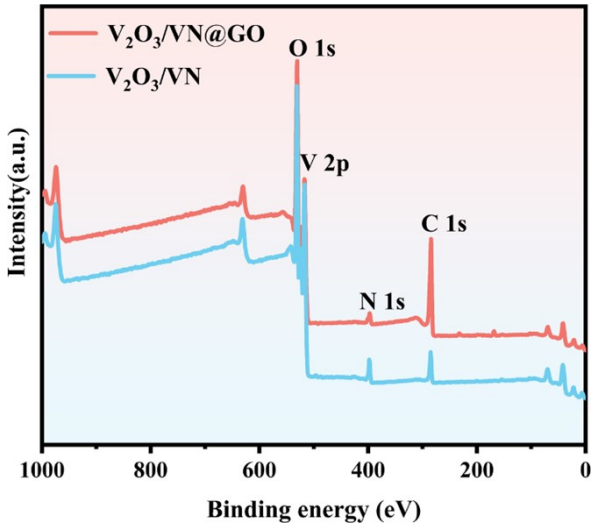

Figure S5. XPS survey spectra of V_2O_3/VN and V_2O_3/VN@GO.

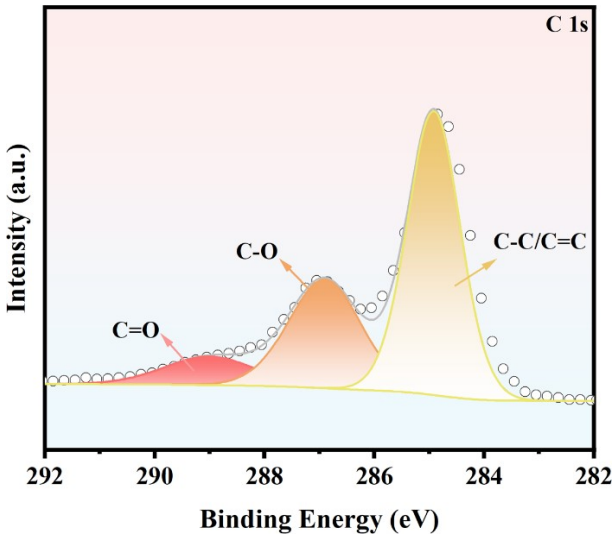

Figure S6. C 1s spectrum of V_2O_3/VN@GO.

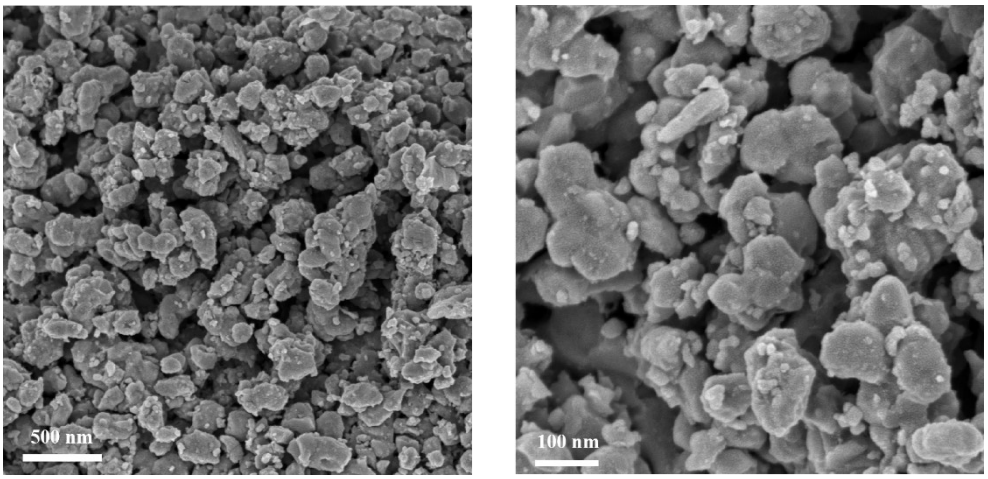

Figure S7. SEM images of V_2O_3/VN.

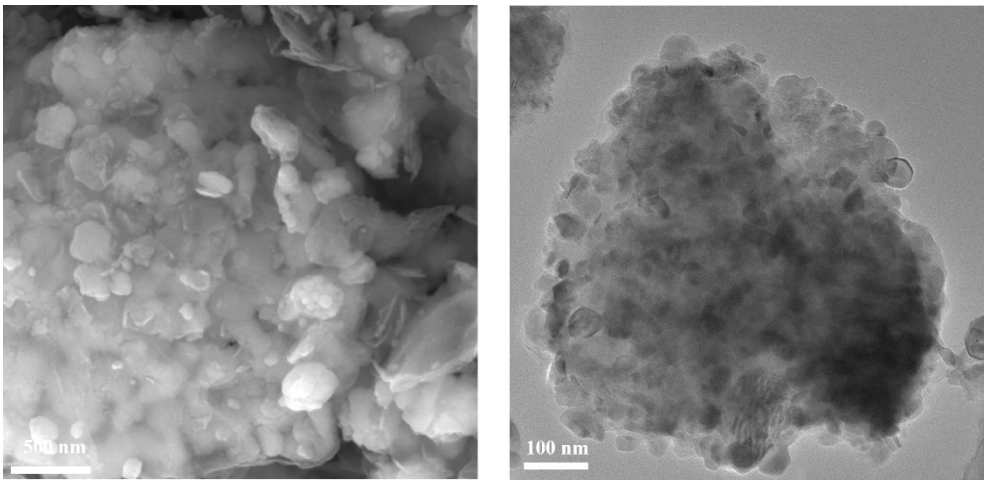

Figure S8. SEM images of V_2O_3/VN@GO.

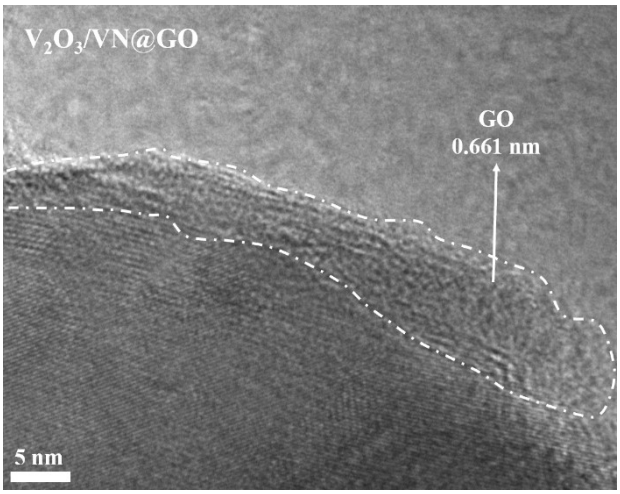

Figure S9. Graphene oxide thickness in TEM images of V_2O_3/VN@GO.

3. Supplementary measurements

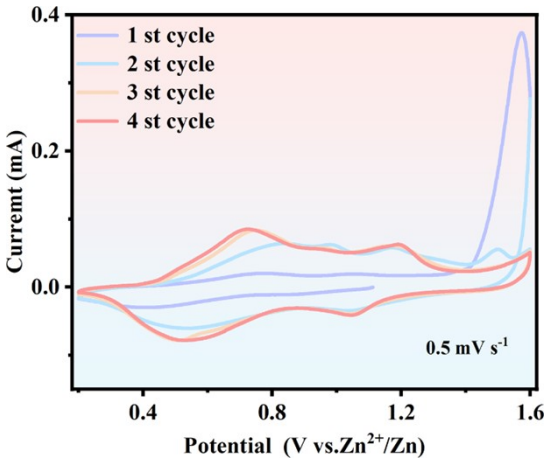

Figure S10. CV curves of V_2O_3/VN at 0.5 mV s^{-1}.

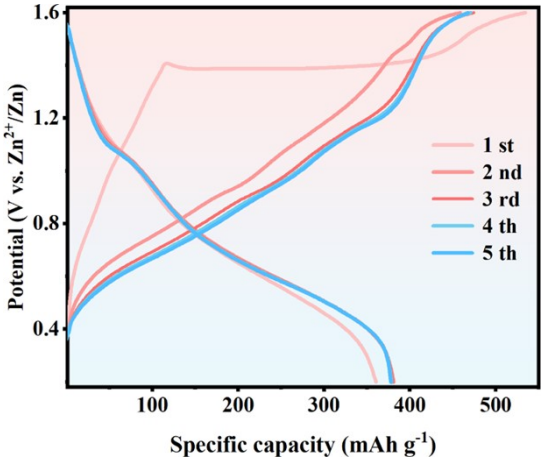

Figure S11. GCD curves of V_2O_3/VN@GO at 0.5 A g^{-1}.

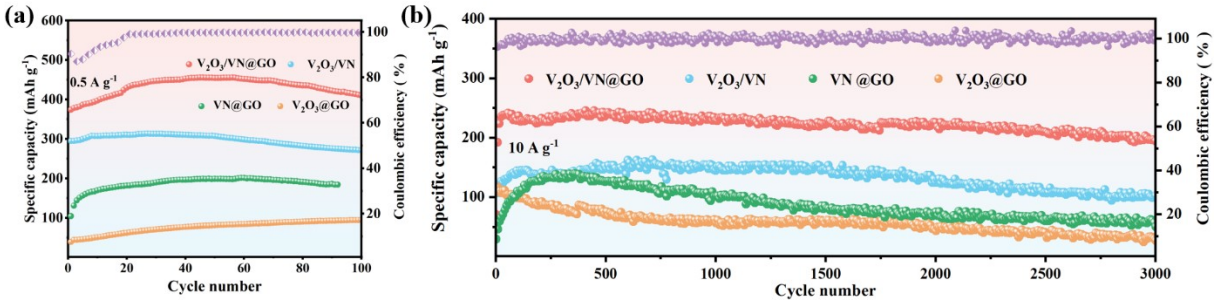

Figure S12. Cycle capacity of V_2O_3/VN@GO, V_2O_3/VN, V_2O_3@GO and VN@GO cathodes at 0.5 A g^{-1} (a) and 10 A g^{-1} (b).

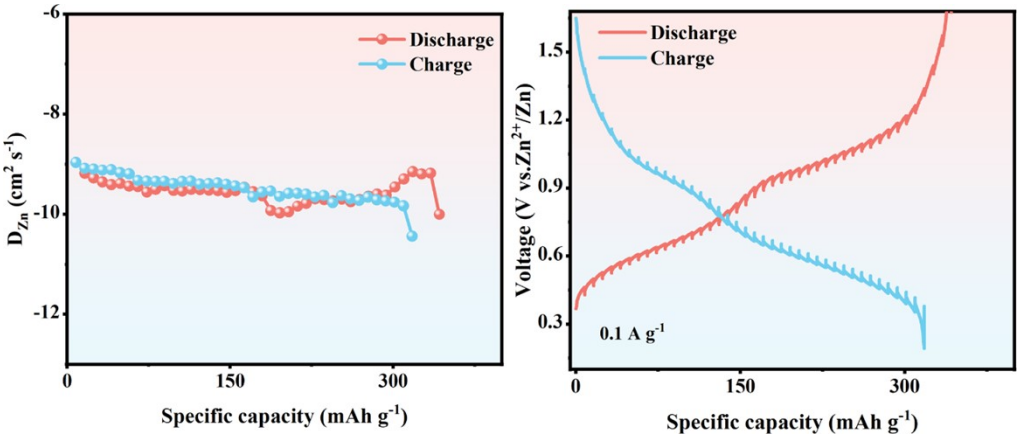

Figure S13. The diffusion coefficients of Zn^{2+} in V_2O_3/VN during charging and discharging processes.

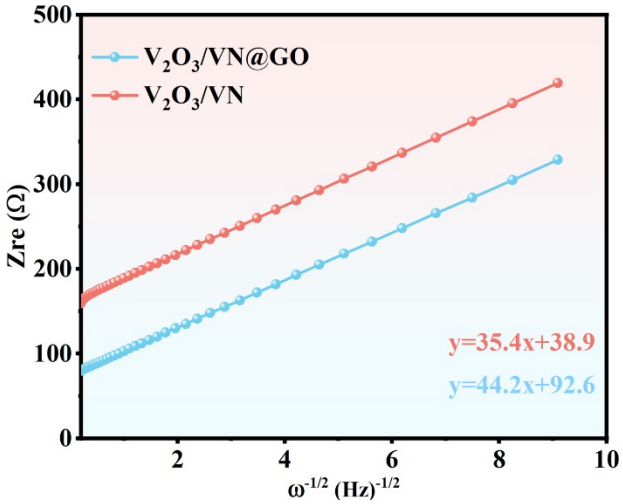

Figure S14. Linear relationship between Z′ and $\omega^{-½}$ of pristine V_2O_3/VN and V_2O_3/VN@GO.

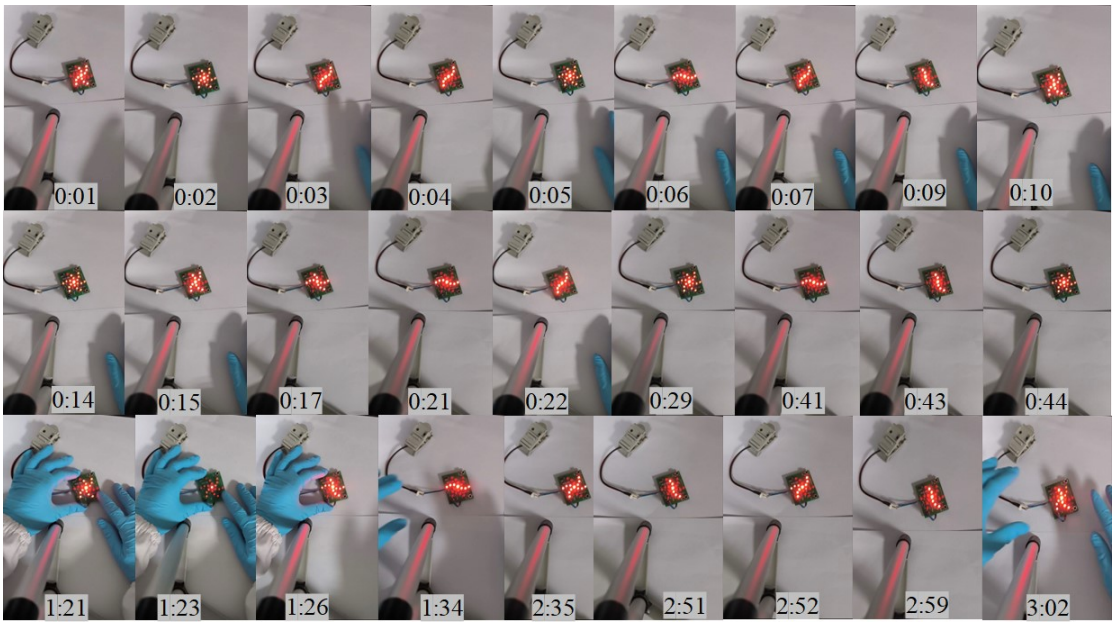

Figure S15. Photograph of connected Zn//V_2O_3/VN@GO batteries powering LED lights.

4. Theoretical calculations

Density functional theory (DFT) calculations were performed using the projector augmented plane-wave method [3] within the Vienna Ab initio Simulation Package (VASP) [4, 5]. The generalized gradient approximation (GGA) was used in the scheme of Perdew-Burke-Ernzerhof (PBE) to describe the exchange-correlation functional [6]. The cut-off energy for plane wave was set to 480 eV. The energy criterion was set to 10^{-4} eV in iterative solution of the Kohn-Sham equation. All the structures were relaxed until the residual forces on the atoms have declined to less than 0.05 eV/Å. To prevent interaction between periodic units in the vertical direction, a vacuum space of 20 Å was employed. A Monkhorst–Pack scheme with a k-points mesh of 3 × 2 × 1 was used. The diffusion barrier of adsorbed hydrogen at different adsorption sites were explored by using the Nudge Elastic Band (CI-NEB) method [7].

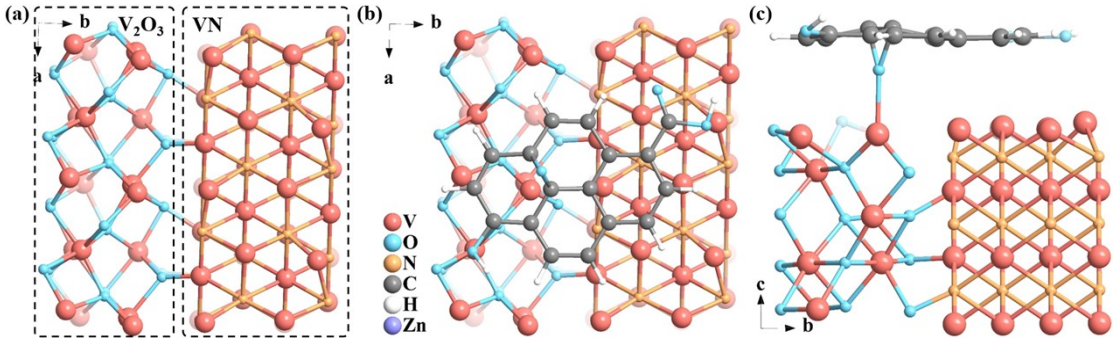

Figure S16. (a) Theoretical models of V_2O_3/VN. Top (b) and side (c) views of the theoretical models for V_2O_3/VN@GO.

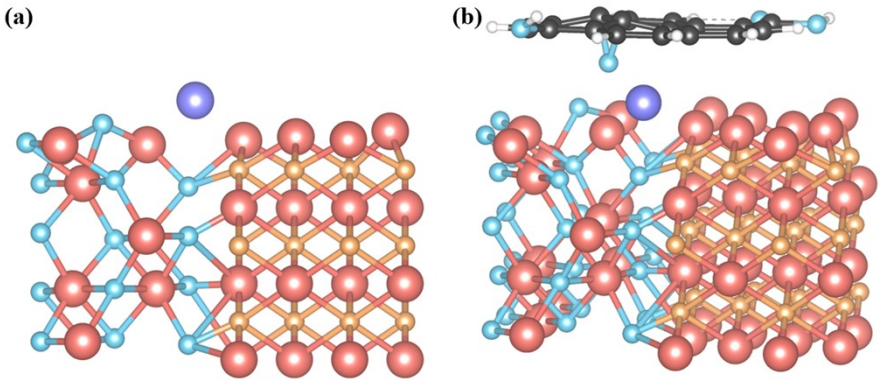

Figure S17. Structural diagrams of Zn^{2+} adsorbed on V_2O_3/VN (a) and V_2O_3/VN@GO (b) cathodes.

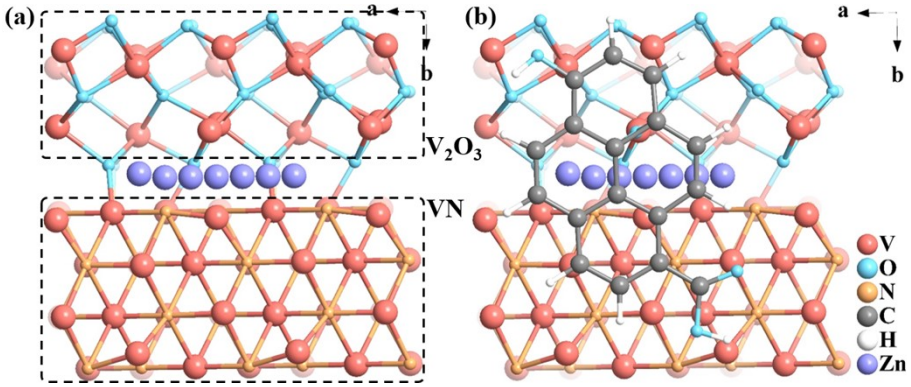

Figure S18. The migration pathways for Zn^{2+} in V_2O_3/VN (a) and V_2O_3/VN@GO cathodes along a-axis.

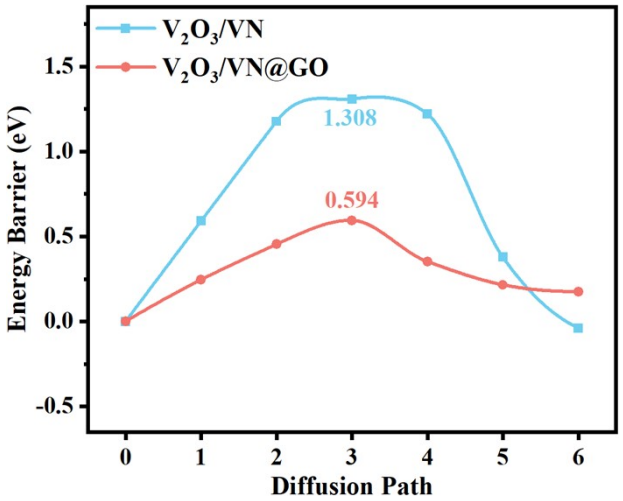

Figure S19. Calculated Zn^{2+} diffusion barriers in V_2O_3/VN@GO and V_2O_3/VN@GO cathodes along a-axis.

5. Zinc ion storage mechanism

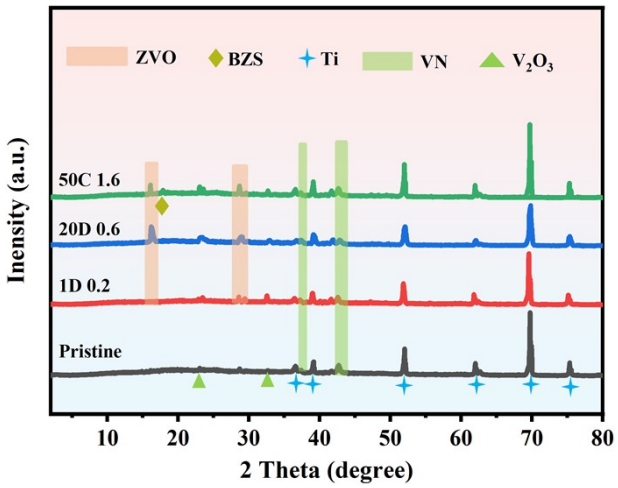

Figure S20. Ex situ XRD patterns after 50 cycles.

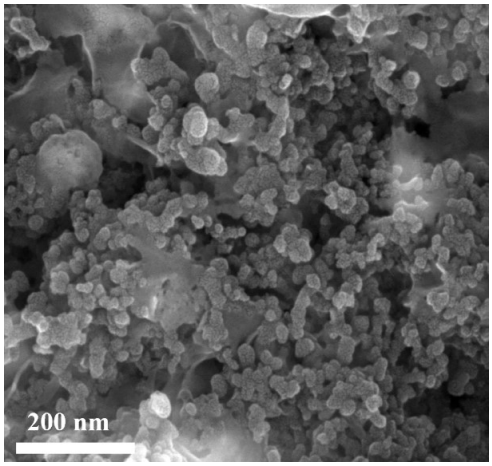

Figure S21. SEM image of V_2O_3/VN@GO electrode discharged to 0.2 V.

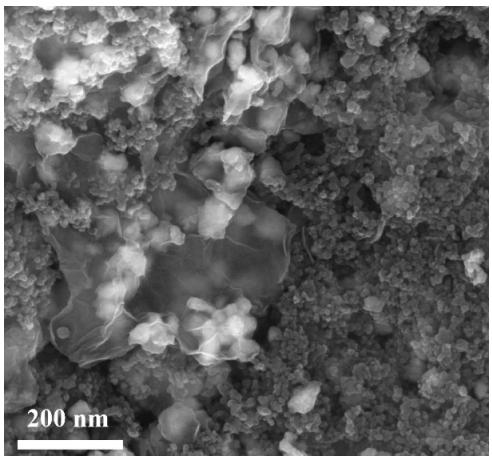

Figure S22. SEM image of V_2O_3/VN@GO electrode charged to 1.6 V.

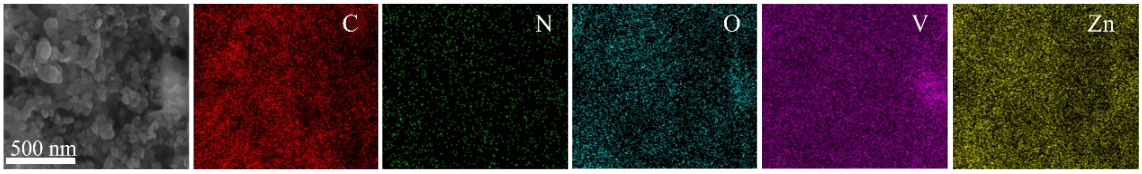

Figure S23. Elemental mapping images of V_2O_3/VN@GO.

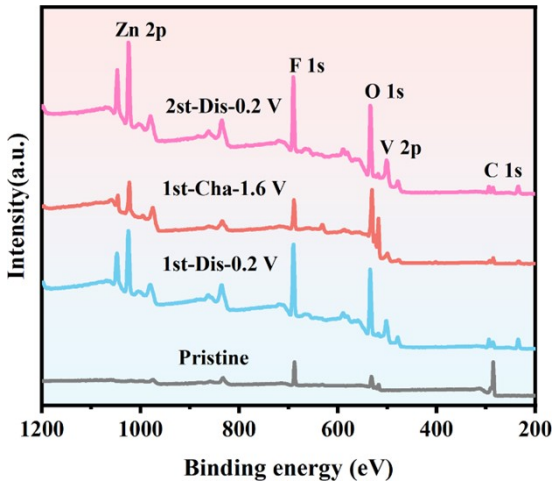

Figure S24. All-elements XPS spectra of V_2O_3/VN@GO at different charging and discharging states.

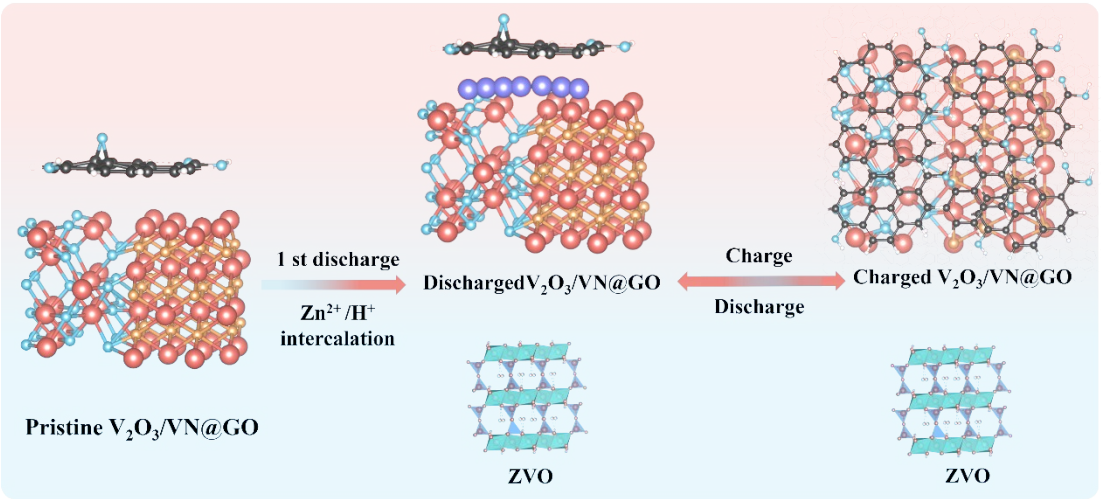

Figure S25. Diagram of Zn^{2+} ion storage mechanism in V_2O_3/VN@GO.

References

[1] J.-P. Cao, Y.-S. Xue, N.-F. Li, J.-J. Gong, R.-K. Kang, Y. Xu, Lewis Acid Dominant Windmill-Shaped V8 Clusters: A Bifunctional Heterogeneous Catalyst for CO_2 Cycloaddition and Oxidation of Sulfides, J. Am. Chem. Soc. 141 (2019) 19487-19497. https://doi.org/10.1021/jacs.9b11146

[2] Y. Liu, C. Gao, Y. Sun, X. Hao, Z. Pi, M. Yang, et al., Enhancing the electrochemical activation kinetics of V_2O_3 for high-performance aqueous zinc-ion battery cathode materials, Chem. Eng. J. 490 (2024) 151535. https://doi.org/10.1016/j.cej.2024.151535

[3] G. Kresse, D. Joubert, From ultrasoft pseudopotentials to the projector augmented-wave method, Phys. Rev. B. 59 (1999) 1758. https://doi.org/10.1103/PhysRevB.59.1758

[4] G. Kresse, J. Hafner, Ab initio molecular-dynamics simulation of the liquid-metal-amorphous-semiconductor transition in germanium, Phys. Rev. B. 49 (1994) 14251. https://doi.org/10.1103/PhysRevB.49.14251

[5] G. G. Kresse, J. J. Furthmuller, Efficient Iterative Schemes for Ab Initio Total-Energy Calculations Using a Plane-Wave Basis Set, Phys. Rev. B. 54 (1996) 11169. https://doi.org/10.1103/PhysRevB.54.11169

[6] J.P. Perdew, Y. Wang, Accurate and simple analytic representation of the electron-gas correlation energy, Physical Review B, 45 (1992) 13244-13249. https://doi.org/10.1103/PhysRevB.45.13244

[7] G. Henkelman, B.P. Uberuaga, H. Jónsson, A climbing image nudged elastic band method for finding saddle points and minimum energy paths, J. Chem. Phys 113 (2000) 9901-9904. https://doi.org/10.1063/1.1329672